Composites Science and Technology 191 (2020) 108071

Contents lists available at ScienceDirect

Composites Science and Technology

journal homepage: http://www.elsevier.com/locate/compscitech

Halloysite nanotubes@polydopamine reinforced polyacrylamide-gelatin hydrogels with NIR light triggered shape memory and self-healing capability

Xiang Cao, Hongzhong Liu, Xiaohan Yang, Jinhuan Tian, Binghong Luo, Mingxian Liu *

Department of Materials Science and Engineering, Jinan University, Guangzhou, 510632, PR China

ARTICLE INFO

Keywords:
Halloysite
Polydopamine
Nano composites
Shape memory performance
Self-healing capability

ABSTRACT

In this study, the polyacrylamide-gelatin composite hydrogels reinforced by halloysite nanotubes@polydopamine (HNTs@PDA) with NIR triggered shape memory performance and self-healing capacity were prepared through in-situ free radical polymerization of acrylamide in the mixture of Laponite-RD, HNTs@PDA and gelatin. HNTs@PDA was firstly synthesized through oxidative polymerization of dopamine on the surfaces of HNTs. HNTs@PDA was characterized by transmission electron microscopy, scanning electron microscopy, Fourier-transform infrared spectroscopy, X-ray diffraction, thermogravimetric analysis, Zeta potential, particle size analysis, and X-ray photoelectron spectroscopy. The photothermal performance of HNTs@PDA was then determined and the results reveal that HNTs@PDA can be employed as a superior photothermal agent to prepare light responsive hydrogels. The structure, morphology, mechanical properties, NIR triggered shape memory performance and self-healing capacity of the composite hydrogels were studied. The modified nanotubes act as cross-linking agent of polyacrylamide to form a rigid network in the hydrogel matrix, which leads to a significant increase in the mechanical properties. Moreover, the NIR triggered shape recovery process of the hydrogel is quite rapid, for example, it is only 63 s for recovering 720° shape change for the hydrogel of HNTs@PDA 40. The maximum NIR triggered healing efficiency of the hydrogels can reach 76%. The HNTs@PDA reinforced hydrogels with superior mechanical properties, NIR triggered shape memory, and self-healing ability exhibit promising applications in biomedical materials and smart engineering materials.

1. Introduction

Hydrogel is a soft material comprising of a crosslinked macromolecular network structure. Attributed to the presence of hydrophilic groups attached to the polymer skeleton and crosslinking network among polymer chains, hydrogels are able to absorb and retain water with high resistance to be dissolved in the water [1]. Therefore, hydrogels show great potential in biomedical [2], agricultural [3], industrial areas [4]. For example, hydrogel can be widely used as tissue engineering scaffolds [5], drug delivery systems [6], wound dressing [7], biosensors [8], and coating for biodevice in biomedical area. Zhao et al. utilized gelatin of porcine skin flexibly to prepare photocrosslinkable gelatin such as gelatin methacrylamide (GelMA) and then developed a photocrosslinkable GelMA hydrogel. This material exhibits good flexibility in biological, degradation, and mechanical properties, which can meet the requirements of formation of epidermis in reconstruction of epidermis and wound dressing [9]. Naumenko et al. developed a chitosan-agarose-gelatin hydrogel doped with clay nanotubes through freeze-dry technology. This composite possesses enhanced mechanical properties, biocompatibility and biodegradability [10]. The composite hydrogel used in tissue engineering scaffolds can also be fabricated by mixing of hyaluronic acid and halloysite [11]. In addition, responsive hydrogels were classified into electromagnetic radiation responsive hydrogels [12], ionic strength-responsive hydrogels [13], temperature responsive hydrogels [14], light responsive hydrogels [15], pH-responsive hydrogels [16] based on the responsiveness to external environment stimuli [17]. In recent years, near-infrared (NIR) irradiation responsive hydrogels attracted numerous attentions, especially for its triggered shape memory and self-healing performance. For instance, Tong et al. developed a double cross-linked network hydrogel composites using acrylamide, gelatin and graphene oxide (GO) as raw material. This hydrogel has the capacity to fix temporary shapes rapidly

* Corresponding author.
E-mail address: liumx@jnu.edu.cn (M. Liu).

https://doi.org/10.1016/j.compscitech.2020.108071
Received 14 December 2019; Received in revised form 12 February 2020; Accepted 13 February 2020
Available online 19 February 2020

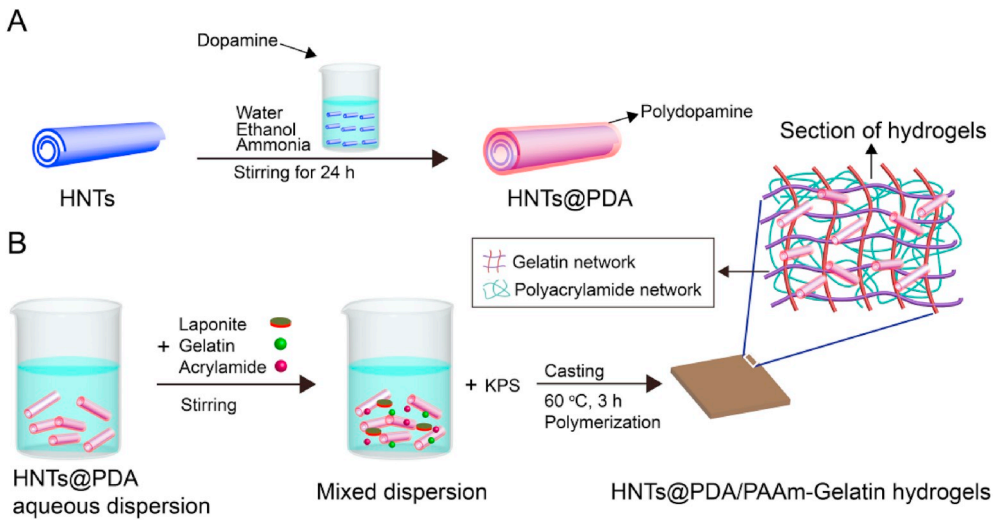

Fig. 1. Schematic illustration for the synthesis of HNTs@PDA (A) and the preparation process of the HNTs@PDA/PAAm-Gelatin hydrogels (B).

through cooling in ice water and is capable of completing shape recovery for nearly 100 s by irradiation using a NIR laser. In this systems, GO is able to transform NIR energy into thermal energy, which promotes the shape recovery of the hydrogel sample [18]. In addition, graphene was used as a photothermal agent to modify hydrogel. Wang et al. constructed a poly (N, *N*-dimethylacrylamide) hydrogel on three-dimensional graphene networks. This material exhibits excellent conductivity, neural compatibility, and NIR triggered photothermal transforming efficiency which leads to the good self-healing performance of the hydrogel [19]. For preparation of NIR responsive hydrogel, it is necessary to incorporate a photothermal agent into the polymer network.

Halloysite nanotubes (HNTs), with chemical formula of $Al_2Si_2O_5(OH)_4{\cdot}nH_2O$, are natural one-dimensional (1D) aluminosilicate clay [20]. HNTs have a generally hollow tubular structure, whose inner diameter, outer diameter, and length ranges 15–30 nm, 50–70 nm, and 100–1500 nm, respectively [21]. The external surfaces of the tubes are mainly composed of silicon-oxygen (Si–O) groups, and the inner surfaces of HNTs consist of aluminoxane (Al–OH) groups [22]. HNTs show many features for application in composite hydrogel such as good biocompatibility, easy chemical modification, low cost, environmentally friendliness, rich pore structure, high aspect ratio, large surface area, high strength, and satisfactory dispersion [23,24]. HNTs are usually employed as nanofillers to reinforce polymers such as rubbers [25], plastics [26], fibers [27], and coatings [28]. Good dispersity arising from the negative zeta potentials of the nanotubes gives them opportunity to improve the mechanical performance and dimensional stability in polymer matrix [29,30]. For example, HNTs were mixed with carboxylated butadiene-styrene rubber (xSBR) through co-coagulation method. The composites possess enhanced mechanical properties especially the tensile modulus and hardness, which can be ascribed to strong interfacial interactions between HNTs and xSBR [31,32]. HNTs have also been utilized to synthesize nanocomposite hydrogels [33,34], and it is proved that HNTs show good dispersion [35] and excellent reinforcement effect [36,37] in polyacrylamide hydrogels [38] and chitosan hydrogels [39]. In addition, HNTs have been developed in biomaterials such as capture of tumor cells [40,41], bone/skin repairing [42,43], and drug controlled release systems [44,45]. Moreover, the hydrophilic lumen of HNTs was used to confined Ca^{2+}-crosslinked alginate network, which are suitable for selective and triggered adsorption and/or drug release [46]. Recently, Panchal et al. utilized self-assembly process to coat HNTs on hair surfaces with different drugs, which are used as medical and cosmetic formulation for hair modification, protection and enhancement [47].

Polydopamine (PDA) has attracted great attentions [48] and has been widely applied in cancer treatment [49], shape memory, and self-healing materials [50]. Because PDA can absorb NIR light energy and transform them into thermal energy with high efficiency. For example, dopamine melanin colloidal nanospheres were synthesized in an alkaline solvent by Lu et al., it was found that PDA displayed superior tumor treatment effect both in vitro and in vivo [51]. Xia et al. utilized PDA particles and poly(vinyl alcohol) to prepare poly(vinyl alcohol) composite hydrogels, and their results suggested that this material possesses ultrafast NIR light triggered shape memory and self-healing capability [52].

In the present work, PDA was coated on the surfaces of HNTs through self-polymerization of dopamine in HNTs dispersion. The prepared HNTs@PDA shows good water dispersion ability and favorable photothermal effect, so HNTs@PDA is readily dispersed in hydrogels matrix. HNTs@PDA was then mixed with Laponite-RD, acrylamide and gelatin to prepare HNTs@PDA/polyacrylamide (PAAm)-gelatin hydrogels via in-situ free radical polymerization of acrylamide. This material exhibits gratifying NIR light triggered shape memory and self-healing behavior. In addition, the shape recovery process of the hydrogel is quite rapid, and the healing efficiency can reach 76%. The mechanical property of the composite hydrogels is considerably enhanced, especially the tensile strength. HNTs@PDA acts as cross-linking agent of the polymer chains to form a rigid network. This work presents a rapid, effective, and easily realized strategy to construct multifunctional composite hydrogels, which shows great potential in soft actuator materials and biomedical fields such as controlled drug delivery systems.

2. Experimental

2.1. Materials

HNTs with high purity were purchased from Guangzhou Runwo Materials Technology Co., Ltd., China. Dopamine hydrochloride, acrylamide (C_3H_5NO, > 99.0%) and gelatin (gel strength: ~240 g Bloom) were obtained from Aladdin bio-chemical technology Ltd., China. Ammonia hydroxide (NH_4OH, 25%) was purchased from Guangzhou chemical reagent factory, China. Anhydrous ethanol (CH_3CH_2OH, ≥99.7%) was used without any treatment. Potassium persulfate (KPS, $K_2S_2O_8$, >99.5%) was acquired from Tianjin baishi chemical co. LTD. Laponite-RD was bought from BYK. Ultrapure water was originated from Milli-Q Integral Water Purification System.

Table 1
Chemical composition of the prepared hydrogels.

Samples	AAm (g)	Gelatin (g)	HNTs@PDA (g)	KPS (g)	H_2O (mL)	Laponite-RD (g)
HNTs@PDA 0	3	10	0	0.6	20	0.2
HNTs@PDA 10	3	10	0.2	0.6	20	0.2
HNTs@PDA 20	3	10	0.4	0.6	20	0.2
HNTs@PDA 30	3	10	0.6	0.6	20	0.2
HNTs@PDA 40	3	10	0.8	0.6	20	0.2

2.2. Preparation of HNTs@PDA/PAAm-gelatin hydrogels

HNTs@PDA was synthesized according to the reference with slight modification [51]. First, 2 g HNTs powder was added to 65 mL pure water in a 250 mL beaker and dispersed uniformly through ultrasonical treatment for 30 min. Then 2 mL ammonia aqueous solution and 40 mL ethanol were dropped in the beaker successively under mild stirring at 30 °C for 30 min. 0.5 g of dopamine hydrochloride was added in a 25 mL beaker, then 10 mL pure water was injected into the beaker to dissolve the dopamine hydrochloride, then this dopamine solution was added in above-mentioned 250 mL beaker finally. The color of the mixture solution turned to light yellow right away and gradually changed to dark brown. The reaction was performed for 24 h to ensure sufficient polymerization of dopamine on the surface of HNTs. The obtained HNTs@PDA dispersion was centrifuged and washed using distilled water for three times.

HNTs@PDA/PAAm-Gelatin hydrogels were prepared according to previous study [18,53]. Firstly, a specified amount of HNTs@PDA was added into 20 mL pure water in a 100 mL beaker and dispersed uniformly by sonication for 30 min. Then 0.2 g of Laponite-RD and 3 g of acrylamide were added into the beaker and stirred for 30 min. Next, 10 g of gelatin was mixed in the mixture and stirred for 5 h to obtain homogenous dispersion. 0.6 g KPS was added into the mixture solution under stirring, finally the solution was injected into a square PTFE mold (10 cm × 10 cm × 2 cm) and the polymerization was allowed to proceed in the oven at 60 °C for 3 h. The synthesis of HNTs@PDA and the preparation process of HNTs@PDA/PAAm-Gelatin hydrogels were summarily shown in Fig. 1. The hydrogels were expressed according to the weight percent of the HNTs@PDA relative to the water. For example, the hydrogel of HNTs@PDA 40 represents that 0.8 g of HNTs@PDA was added into 20 mL pure water. Chemical composition of the prepared hydrogels is shown in Table 1.

2.3. The shape memory process

The shape memory behavior triggered by NIR light was performed according to literature [18]. Typically, the prepared hydrogels were cut into a strip with a dimension of (length, width, thickness) 35 × 5 × 2 mm. Afterwards, the strip was put in 80 °C water in a Petri dish for 10 s and then twist into a tight helix, subsequently it was immersed in ice water for 30 s to fix the temporary shape. Then a NIR laser (2.0 W/cm^2, 808 nm, 5 mm × 5 mm spot) was used to irradiate the hydrogel strip from top to bottom and the shape recovery process of the hydrogel strip was recorded by a video camera. The speed of shape recovery process was evaluated by the recovered angle. An 808 nm fiber-coupled laser (MD–III–808, Changchun New Industry Optoelectronic Technology Ltd., China) was used to irradiate the hydrogel samples and its output power was 2 W/cm^2.

The shape memory property of the hydrogels was also expressed through patterning with a multi-circle mold. First, the hydrogel piece was put in 80 °C water in a beaker for 10 s and printed with a multi-circle mold. Thereafter, the patterned hydrogel was immersed in ice water in another beaker for 30 s to fix the temporary shape. The hydrogel piece was irradiated at a certain area by NIR laser to observe the shape recovery process.

Another shape memory phenomenon was observed through transforming the hydrogel into a petal. The tailored hydrogel sample was first immersed into 80 °C water in a Petri dish for 10 s and then deformed into a petal shape. The hydrogel sample with petal shape was fixed in ice water for 30 s. Ultimately, a NIR laser was employed to irradiate the petal sample and proceed shape recovery process.

2.4. The self-healing behavior

To study the self-healing performance of HNTs@PDA/PAAm-Gelatin hydrogels, a hydrogel strip with dimension of 30 mm × 5 mm × 2 mm was cut into two pieces. Afterwards, the cut surfaces were immediately brought into together, and the NIR light (output power: 2 W/cm^2) was used to irradiate the hydrogel sample for 3 min to heal the damaged hydrogel. The damaged and healed surfaces were observed by a polarized optical microscope (BX51, Olympus Corporation, Japan). Subsequently, tensile tests were conducted in original state and healed state of the hydrogel with a universal testing machine (UTM- Q422, China Chengde Jinjian Testing Instrument Co., Ltd., China). The tensile speed was set as 50 mm/min.

2.5. Characterizations

2.5.1. Transmission electron microscopy (TEM)

Aqueous dispersions of HNTs and HNTs@PDA (0.05 wt%) were dropped onto a carbon membrane supported copper grid. Transmission electron microscope (JEM-2100F, JEOL Ltd., Japan) was used to observe the morphology at an accelerating voltage of 100 kV.

2.5.2. Scanning electron microscope (SEM)

The surface of HNTs, HNTs@PDA, and the freeze-dried hydrogels was observed by a SEM machine (Zeiss Ultra 55 SEM, KYKY Technology Co., LTD, Germany). And the cross-section morphology of the freeze-dried hydrogels was examined using another SEM machine (TM3030, Hitachi Ltd., Japan). The samples surfaces were sputter-coated with gold film before SEM observation.

2.5.3. Fourier transform infrared spectroscopy (FTIR)

FTIR spectra of HNTs, HNTs@PDA, gelatin, and the freeze-dried hydrogels were measured by a Thermo FTIR (Nicolet iS50, Thermo Fisher Scientific Ltd., USA). The spectra were recorded from 4000 to 400 cm^{-1}.

2.5.4. X-ray diffraction (XRD)

A X-ray diffraction (Rigaku, Miniflex600, CuKα, Japan) was employed to determine the XRD pattern of HNTs powder, HNTs@PDA powder, gelatin, and the freeze-dried hydrogels with a scanning speed of 10°/min ranging from 5 to 70° at an accelerating voltage of 40 kV and the current of 40 mA.

2.5.5. Thermogravimetric analyzer (TGA)

The thermal stability of HNTs and HNTs@PDA was analyzed by TGA machine (TGA2, METTLER TOLEDO, Ltd., Switzerland) from 30 to 800 °C at a heating rate of 10 °C/min under a N_2 atmosphere.

2.5.6. X-ray photoelectron spectrum (XPS)

XPS instrument (ESCALAB250Xi, Thermo Fisher Scientific Ltd., USA) was employed to conduct elemental analysis. The atoms of C, N, O, Al and Si of HNTs and HNTs@PDA were detected.

2.5.7. Zeta potential and particle size analysis

0.05 wt% HNTs and HNTs@PDA aqueous dispersion were prepared

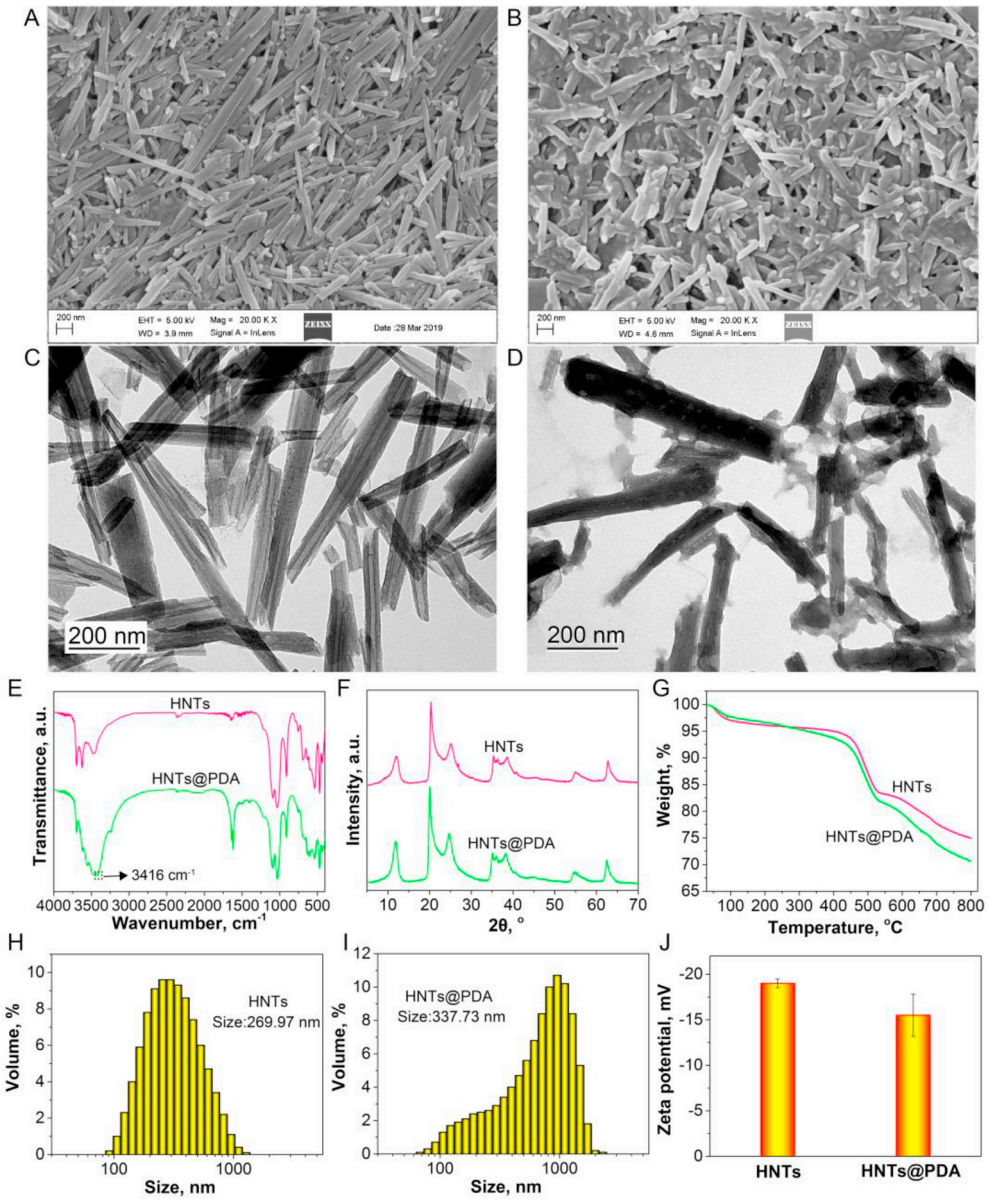

Fig. 2. SEM images of (A) HNTs and (B) HNTs@PDA. TEM images of (C) HNTs and (D) HNTs@PDA. (E) IR, (F) XRD and (G) thermogravimetric curves of HNTs and HNTs@PDA. Particle size distribution of (H) HNTs and (I) HNTs@PDA. (J) Zeta potential of HNTs and HNTs@PDA.

and used to test the zeta potential and particle size distribution by a Zetasizer Nano ZS (Malvern Instruments Co., U.K.).

2.5.8. Photothermal performance of HNTs@PDA and HNTs@PDA/PAAm-gelatin hydrogels

The photothermal performance of HNTs@PDA was evaluated through the following method [54]. First, 1.5 mL HNTs@PDA dispersion was injected into 2.0 mL Eppendorf (EP) tube and concentration gradient was set from 1 to 10 mg/mL. The NIR laser was used to irradiate the sample for 10 min, and laser power density was set as 1.0, 1.5, and 2.0 W/cm^2. The temperature of the sample was recorded immediately with an infrared camera (TiS 55, Fluke Electronic Instrument Ltd., USA) every 60 s while starting irradiation, an infrared photograph was taken every 2 min at the same time. The control group was conducted in pure water under the same test condition. To evaluate the photothermal performance of HNTs@PDA/PAAm-Gelatin hydrogels, a piece of hydrogel was irradiated by the NIR laser (2.0 W/cm^2) and the temperature of the hydrogel was recorded using the infrared camera every 10 s once the irradiation started.

2.5.9. Mechanical properties determination

The universal testing machine (UTM-Q422, Chengde Jinjian Testing Instrument Co., Ltd., China) was used to determine the tensile properties of the hydrogels. The tensile rate was set as 50 mm/min. The hydrogel samples were cut into a strip with a dimension of 30 × 5 × 2 mm before experiment.

2.5.10. Rheological behavior

The dynamic viscosity of HNTs@PDA/PAAm-Gelatin hydrogels was tested by a rotating rheometer (Kinexus pro +, Malvern Instruments, Malvern, UK.) using a parallel plate model with a diameter of 20 mm at room temperature and the thickness of the hydrogel samples was 2 mm. The strain sweep was conducted from 0.1% to 500% at fixed angular frequency of 1 Hz and the frequency sweep was performed from 0.1 to 100 Hz at fixed strain of 0.5%.

2.5.11. Swelling behavior

The swelling property of the hydrogels composite was tested at room temperature for 96 h using deionized water as solvent. The swelling

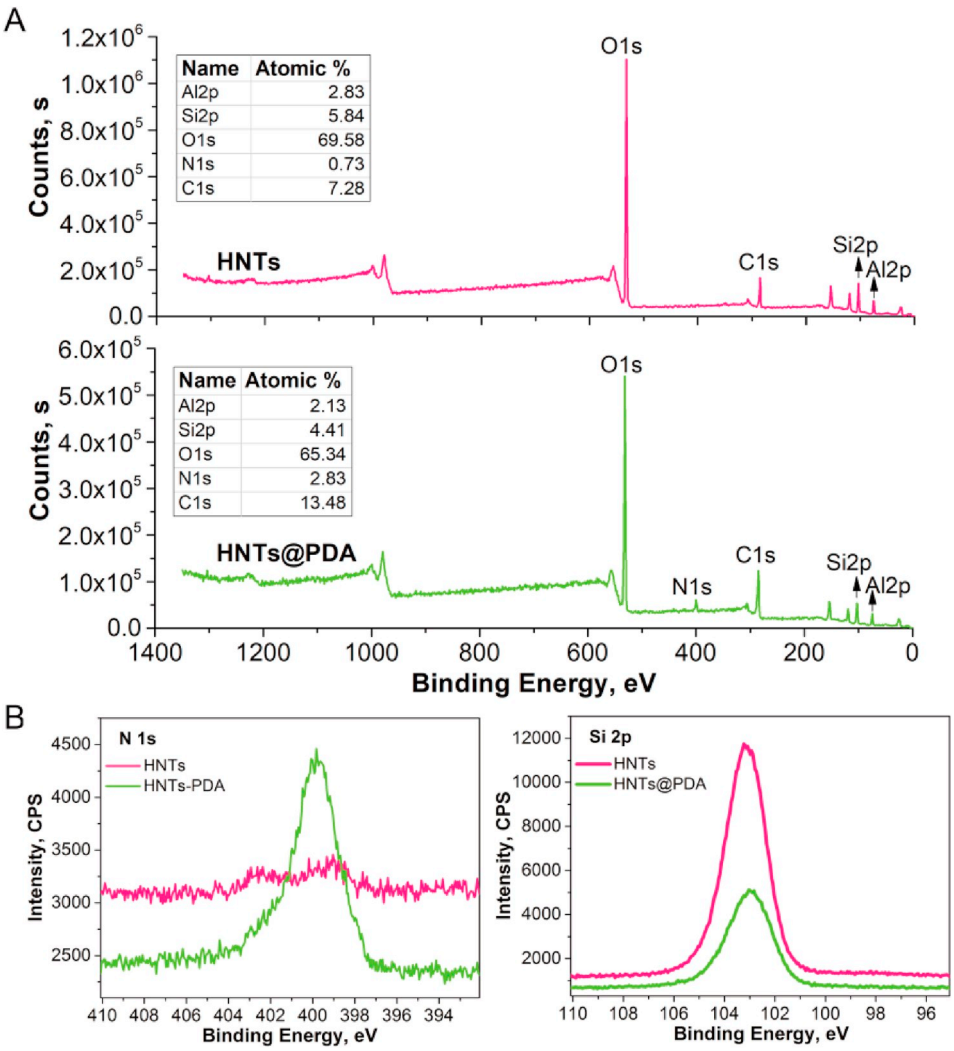

Fig. 3. The survey of (A) XPS spectra of HNTs and HNTs@PDA and (B) high-resolution scanning of nitrogen and silicon for HNTs and HNTs@PDA.

ratio was calculated according to the following formula.

$$\text{Swelling ratio} = (M_1\text{-}M_0)/M_0 \times 100\%$$

Where, M_0 was the initial mass of the sample, and M_1 was the mass of the sample after soaking in water.

3. Results and discussion

3.1. Characterization of HNTs@PDA

HNTs with high surface negative charge and the repulsion interaction endows them excellent water dispersibility, which can be employed to load PDA which possesses photothermal performance and then to prepare composite hydrogels [51,55]. HNTs@PDA was synthesized through the polymerization of dopamine on the surface of HNTs. After the polymerization of dopamine, the color of the solution turns into dark quickly. This results in a PDA layer around the surfaces of HNTs. The dopamine is oxidized and polymerized into PDA, and a crosslinked polymer structure is formed. The polymerization occurs in alkaline condition with the presence of oxygen, so the product is complicated. The molecular weight (or polymerization degree) of the crosslinked PDA was hard to measure [56,57]. The morphology of HNTs and HNTs@PDA was characterized by SEM and TEM. It is obvious that HNTs have sharp and smooth walls in Fig. 2A, while the edges of HNTs@PDA become indistinct and the surfaces are rough in Fig. 2B. This suggests that HNTs@PDA was obtained through warping of PDA layer on HNTs. It also can be seen from Fig. 2C that HNTs show the hollow tubular structure and the surfaces of the tube are clear. After polymerization of dopamine in HNTs dispersion, it is evidenced that the outer surfaces of the tubes are covered with a polymer layer in 2–5 nm thickness for the HNTs@PDA. The diameter, width, and length of the tubes in HNTs@PDA increase compared with the raw HNTs. This also proves that PDA successfully wrapped on the surfaces of HNTs. Fig. 2E compares the FTIR spectra of HNTs and HNTs@PDA. HNTs show hydroxyl group absorption peaks at 3697 cm^{-1} and 3622 cm^{-1} which are assigned to O–H groups in inner-surface and inner hydroxyl groups, respectively [58]. Compared with raw HNTs, the characteristic absorbance of HNTs@PDA at 3693 cm^{-1} and 3620 cm^{-1} are also present, while the synthesized HNTs@PDA shows a new sharper absorbance peak at 3416 cm^{-1} which is attributed to the *N*–H stretching vibration of PDA [51]. This result indicates that dopamine monomer is successfully polymerized on the surfaces of HNTs. The crystal structure of HNTs and HNTs@PDA was identified by XRD. As displayed in Fig. 2F, there is no new diffraction peak which indicates that there is no change in the crystal structure although the warping of PDA on HNTs. This happens because that PDA is amorphous [59]. The TGA curves (Fig. 2G) show that the remaining weight of HNTs is 74.95% while the residue of HNTs@PDA is 70.66%. The weight loss of HNTs is mainly ascribed to the loss of adsorbed water and hydroxyl dehydration. For HNTs@PDA, apart from the evaporation of water and dehydration of hydroxyl, there was

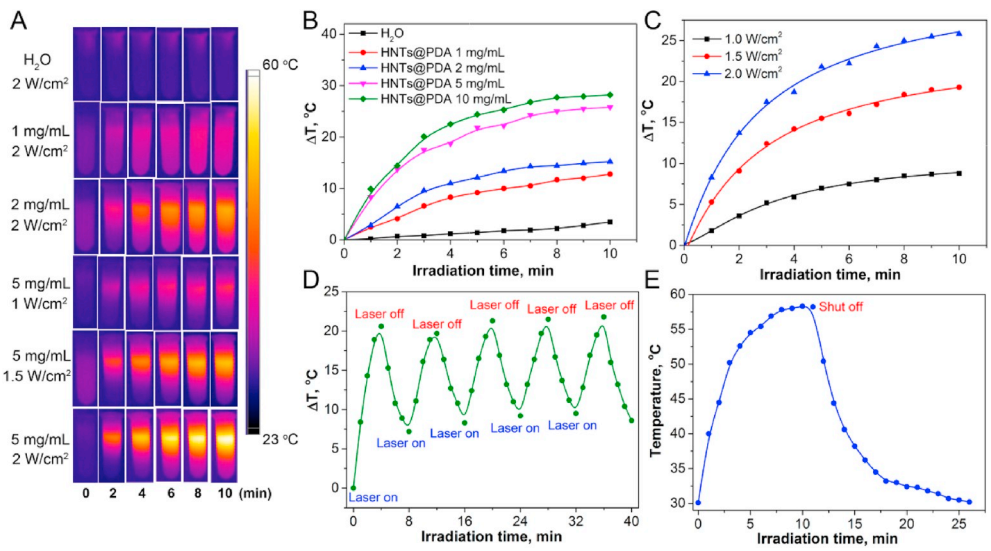

Fig. 4. (A) Photothermal images of HNTs@PDA dispersion under irradiation of 808 nm by infrared camera. (B) Temperature curves of HNTs@PDA dispersion irradiated by an 808 nm laser (2 W/cm^2). (C) Temperature curves of HNTs@PDA solution irradiated by an 808 nm laser with various powers. (D) Temperature change of HNTs@PDA dispersion irradiated by an 808 nm laser (2 W/cm^2) for five cycles. (E) The photothermal response of the HNTs@PDA dispersion for 11 min with an 808 nm laser (2 W/cm^2) and then the laser was turned off.

the decomposition of PDA attached on the surfaces of HNTs. Therefore, the remaining weight of HNTs@PDA is less than the residue of HNTs. The amount of PDA in HNTs@PDA is 4.29 wt% calculated from the TGA results and this result also confirms that PDA successfully warpped on the surfaces of the tubes. Fig. 2H and I show the particle size distribution of HNTs and HNTs@PDA. The average size of HNTs is 269.97 nm, while the average size of HNTs@PDA is 337.73 nm. The increase in size is also due to the wrapping of PDA around HNTs. The zeta potential measurement was carried out to determine the charge properties of the HNTs and HNTs@PDA. The amino groups of PDA are positively charged, so the electrostatic interactions between PDA and negatively charged HNTs lowered the zeta potential of HNTs. The zeta potential value of HNTs and HNTs@PDA dispersions is −19.0 and −15.5 mV in Fig. 2J, respectively. This suggests that both HNTs and HNTs@PDA have good dispersion ability in water, which indicates that HNTs@PDA is able to reinforce the hydrogels.

XPS scanning was conducted on HNTs and HNTs@PDA to further confirm that the presence of PDA layer on HNTs. Fig. 3A and B exhibit the survey of XPS for HNTs and HNTs@PDA and the high-resolution XPS spectra of nitrogen and silicon element. The C 1s peak of carbon element of HNTs is ascribed to the impurities of the HNTs [60]. There is a new peak at 400.1 eV of binding energy in the survey of XPS spectra of HNTs@PDA compared with that of HNTs. The new peak is assigned to the N 1s peak of nitrogen element. The high-resolution XPS spectra shows that the peak of nitrogen of HNTs@PDA becomes stronger than that of HNTs and the peak of silicon of HNTs@PDA is weaker than that of HNTs. This phenomenon suggests that the elements content of the two samples changes significantly and reveals that PDA wrapped on the surface of HNTs successfully.

As showed in Fig. 4, the photothermal performance was determined through recording the temperature of the HNTs@PDA dispersion under NIR light irradiation with an infrared camera. It can be seen from Fig. 4A–C that pure water has a little temperature change while the temperature of all HNTs@PDA dispersion samples increases significantly with the increase in irradiation time, and the temperature rises more rapidly with the increasing in the concentration of HNTs@PDA and laser power. For example, the temperature of HNTs@PDA dispersion was increased by 28.2 °C at a concentration of 10 mg/mL after 10 min irradiation, but the temperature of pure water rose by only 3.5 °C. Fig. 4D demonstrates that the photothermal effect of HNTs@PDA is reversible and stable, since the temperature of HNTs@PDA dispersion changed linearly when the NIR laser was turned on/off for 5 times repeatedly. Fig. 4E illustrates the real-time temperature change behavior of HNTs@PDA dispersion under the NIR light irradiation for 11 min and then the laser was turned off. All the results suggest that HNTs@PDA can be used as an excellent photothermal agent to prepare light responsive hydrogels.

3.2. Characterization of HNTs@PDA/PAAm-gelatin hydrogels

HNTs@PDA exhibits good dispersion ability in water and photothermal effect, which can be used as a photothermal agent to reinforce

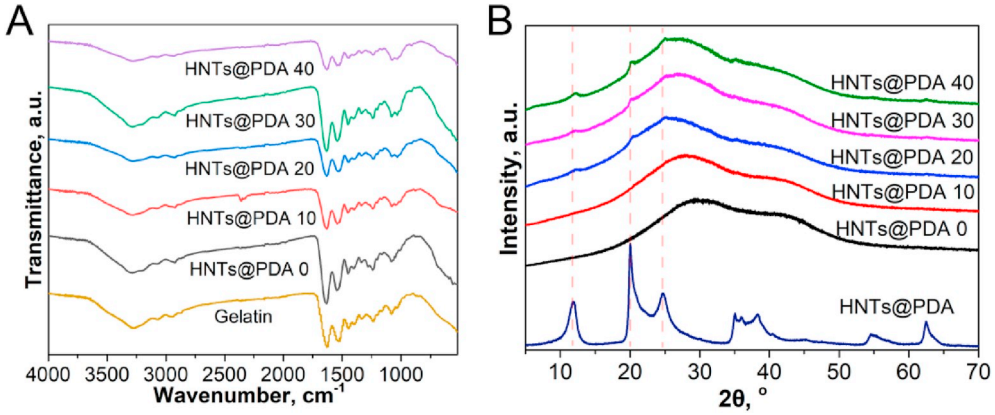

Fig. 5. IR (A) and XRD (B) of hydrogels with different HNTs@PDA contents.

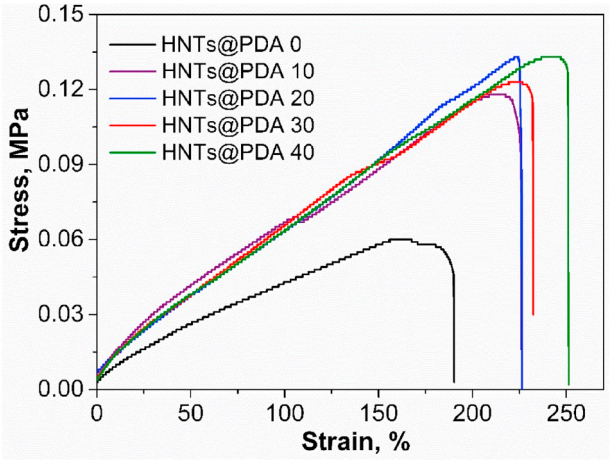

Fig. 6. Stress-strain curves of hydrogels with different HNTs@PDA contents.

hydrogels. Laponite-RD, acrylamide, gelatin, and HNTs@PDA were uniformly mixed and then potassium persulfate was used as initiator to prepare composite hydrogels via in-situ free radical polymerization of acrylamide. Gelatin is incorporated into the PAAm hydrogel for achieving shape-memory property. FTIR spectra and XRD pattern of the hydrogels were determined and as shown in Fig. 5. It can be seen from Fig. 5A that the IR of the HNTs@PDA/PAAm-Gelatin hydrogels are extremely similar to that of gelatin, the characteristic peak of amide-I related to the stretching vibration of N–H appears at a wavenumber of 3278 cm^{-1} for gelatin and the composite hydrogels. The absorption peaks at 1628 cm^{-1} for all samples are attributed to the C═O stretching vibration which corresponds to the amide-I peak primarily. And the O–H asymmetric stretching vibration was detected at wavenumbers of 1030 cm^{-1} for all samples [61]. As a result of the high content of gelatin (See Table 1), the characteristic peaks of HNTs@PDA and PAAm are hided. Fig. 5B shows the XRD pattern of HNTs@PDA and the wet hydrogels. It is clear that the peaks located at 12° (001 plane), 20° (020 plane), 25° (002 plane) assigned to 7, 4.4 and 3.5 Å basal reflections of HNTs remain in the HNTs@PDA/PAAm-Gelatin hydrogels, indicating that the interlayer spacing and crystal structure of HNTs do not change [38,62]. The long PAAm and gelatin chains cannot enter interlayer of the tubes. Previous study also indicated that PAAm was located on the outer or inner surfaces of the tubes but not in the layer spacing [53]. No diffraction peaks of HNTs appear in the XRD pattern of HNTs@PDA 10, which is caused by the low content of HNTs@PDA.

HNTs show high aspect ratios and mechanical strength (elastic modulus ~130 GPa), so they can effectively enhance the strength of PAAm hydrogel [38,53]. Fig. 6 shows the stress-strain curves of hydrogels with different HNTs@PDA contents. It is clear that the tensile strength of the composite hydrogels is higher than that of the hydrogels without HNTs@PDA. The tensile strength of the neat hydrogel is only 0.060 MPa. In contrast, the tensile strength of the hydrogel of HNTs@PDA 10 is 0.118 MPa and it is 0.133 MPa when the HNTs@PDA content is 40 mg/mL, which is 1.97 and 2.22 multiples of the neat hydrogel, respectively. This can be understood by the formation of a rigid network in PAAm-gelatin hydrogel matrix at relatively high loading. The rigid inorganic network can decrease the flexibility of dual network structure of the PAAm-gelatin hydrogel and toughen the hydrogels. The good dispersibility of the tubes and interfacial interactions between the tubes and polymer chains account for the increase of the mechanical performance [55]. Furthermore, the hydrogen bond can be formed between silanol of HNTs and amide groups of PAAm [38]. Because the layer of PDA on HNTs is thin and the content is low, HNTs@PDA is also able to interact with the hydrogel by hydrogen bond interactions. It can be observed from the SEM result below that HNTs@PDA is well dispersed in the PAAm-gelatin matrix. Besides, a

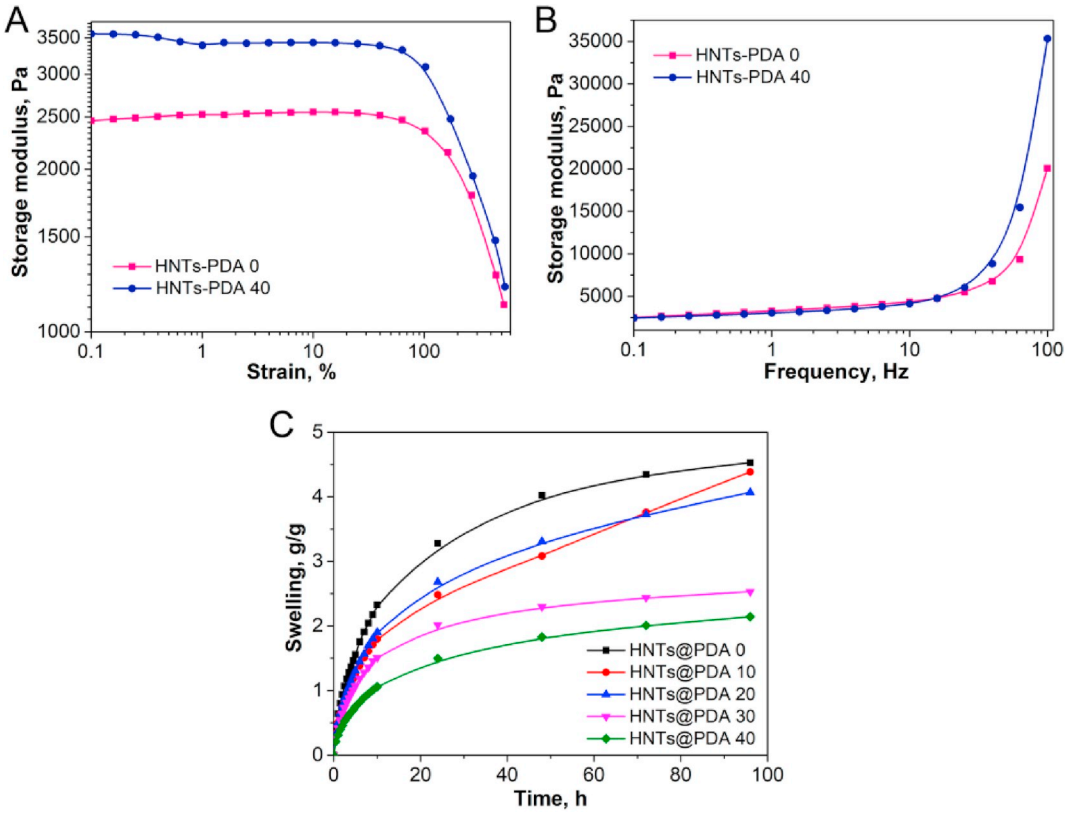

Fig. 7. Rheological properties of HNTs@PDA/PAAm-Gelatin hydrogels with different HNTs@PDA contents. Storage modulus as a function of strain from 0.1% to 500% (A) and angular frequency from 0.1 to 100 Hz (B). (C) Swelling ratio of HNTs@PDA/PAAm-Gelatin hydrogels with different HNTs@PDA contents.

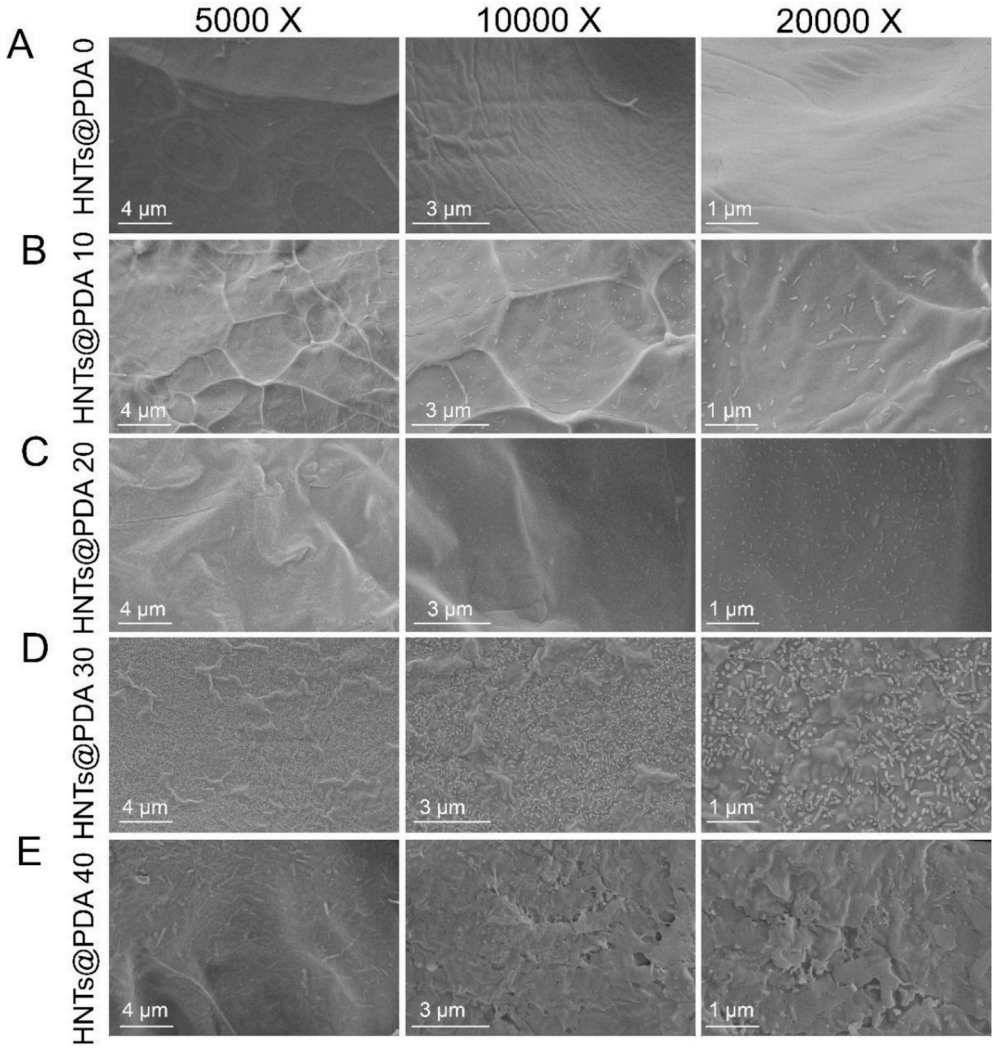

Fig. 8. SEM images of hydrogels with different HNTs@PDA contents.

inorganic/organic hybrid network was formed through the interactions between the Laponite-RD and the hydrogels such as hydrogen bonding and/or ionic interaction [63]. As a consequence, Laponite-RD also promotes the formation of cross-linked network and increases mechanical properties of the composite hydrogels.

Dynamic viscoelastic properties of HNTs@PDA/PAAm-Gelatin hydrogels as a function of strain and frequency were further investigated using a rheometer. Fig. 7A shows that the storage modulus of the samples decreases with increasing strain while the storage modulus substantially increases with the addition of HNTs@PDA. For example, the storage modulus of the hydrogel of HNTs@PDA 40 (3392.7 Pa) at 1% strain is greater than that of the hydrogel without HNTs@PDA (2527.7 Pa). Fig. 7B displays the storage modulus curves with frequency sweep of the hydrogel. It is clear that the storage modulus of the hydrogel of HNTs@PDA 40 (35323 Pa) at 100 Hz is also higher than that of the neat hydrogel (20076.8 Pa). These results also show that HNTs@PDA has an acceptable reinforcing ability towards hydrogels.

Evidently, the swelling ratio of the hydrogel composites can be influenced by the HNTs@PDA content. The swelling behavior of the hydrogel composites was determined through soaking them in deionized water. As displayed in Fig. 7C, the swelling ratio of the neat hydrogels is higher than that of the composite hydrogels with HNTs@PDA. The swelling ratio decreases with the increase of HNTs@PDA content, for example, when soaking in deionized water for 96 h, the swelling ratio of the neat hydrogel (4.53) is 2.12 multiples of the hydrogel of HNTs@PDA 40 (2.14). This can be understood by the decreased polymer component content in the composite hydrogels, while the inorganic HNTs@PDA has relatively low swelling ratio in water.

To further illustrate the existence of HNTs@PDA on the surface of hydrogels, the microstructure of hydrogels was examined by SEM. Fig. 8 shows SEM images of hydrogels with different HNTs@PDA contents. It can be seen that no HNTs@PDA is found on the surface of neat hydrogels, but there are HNTs@PDA in the surfaces of HNTs@PDA/PAAm-Gelatin hydrogels and the distribution is more concentrated as the increase in the content of HNTs@PDA. HNTs@PDA exhibits an excellent dispersion state and good interfacial bonding with the matrix, which is associated with the special aspect ratios and superior water dispersibility of the tubes. Owing to the content of HNTs@PDA is too high, it is obvious that the nanotubes in the hydrogel of HNTs@PDA 40 are slightly aggregated. The nanotubes are well embedded into the PAAm gel matrix, which contributes to the enhancement of the hydrogel performance. In addition, atomic force microscope (AFM) also can be performed to investigate the influence of HNTs on the performance of hydrogels [10].

Fig. 9 displays the SEM images of cross-section morphology of neat hydrogel and HNTs@PDA/PAAm-Gelatin hydrogels. It is not difficult to find that the pore size of the hydrogel ranges from 100 to 300 μm. As the increase in HNTs@PDA content, the pore size of the hydrogels decreases. The water in hydrogel is expected to fill the space between the polymer chains. Due to the presence of HNTs@PDA, hydrogel undergoes

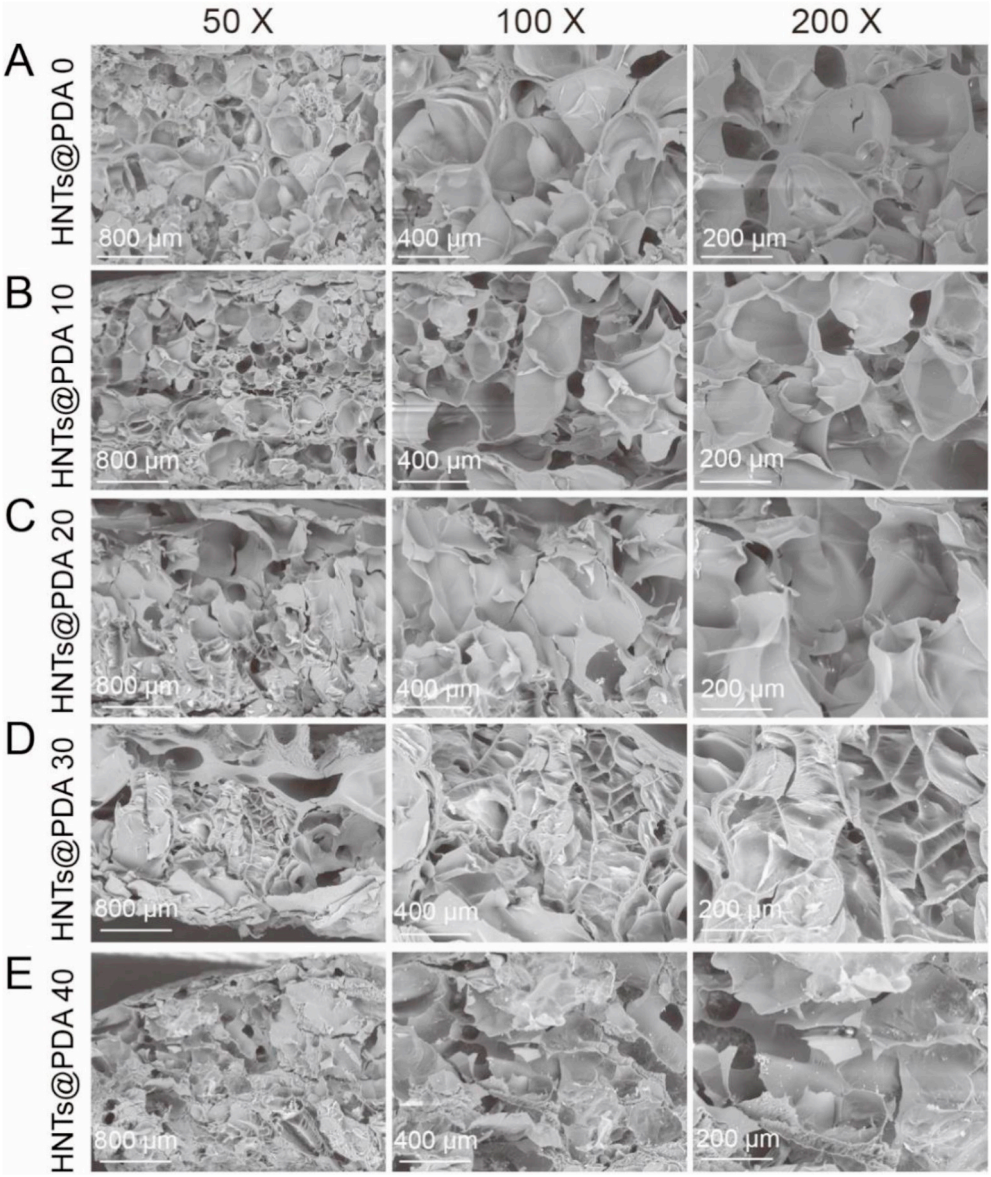

Fig. 9. SEM images of cross section of hydrogels with different HNTs@PDA contents.

phase separation during the freeze-drying process and water plays the role of porogenic agent. As a consequence, the water content of the composite hydrogels at same volume decreases and the pore size of HNTs@PDA/PAAm-Gelatin hydrogels is smaller than that of the neat hydrogel. It is assumed that HNTs@PDA can increase the mechanical properties of the hydrogels by virtue of the decrease of the pore size [39].

3.3. The shape memory performance

The twist model was examined under the NIR light irradiation to study the shape-memory performance of HNTs@PDA/PAAm-Gelatin hydrogels. Fig. 10A and B show the shape recovery process of hydrogels. The hydrogel without HNTs@PDA recovers hardly even after 240 s NIR light irradiation. This indicates that neat hydrogels are capable of keeping the temporary shape well at room temperature and it is because the gelatin in hydrogels possesses the cooling-fixed shape-memory property [18]. In contrary, the hydrogel of HNTs@PDA 40 recovers quickly under the NIR light irradiation and it can complete the shape recovery process only for 220 s. In the present study, the shape recovery process was recorded with a video camera (Video S1) and the shape-recovered angle (θ) at corresponding time was measured from the captured video. The θ as a function of NIR irradiation time is employed to compare the shape-memory capability of the hydrogels. It can be observed from Fig. 10C that the hydrogel without HNTs@PDA can maintain its temporary shape and cannot return to its permanent shape, but the hydrogel of HNTs@PDA 40 recovers fast. The hydrogel containing more HNTs@PDA returns to its permanent shape faster. For instance, when the θ is 720°, it is required to take 63 s for the hydrogel of HNTs@PDA 40, and the time is increased to 80 s and 107 s for the hydrogel of HNTs@PDA 30 and HNTs@PDA 20, respectively. However, the neat hydrogel only recovers 30° after 218 s NIR light irradiation, and the hydrogel of HNTs@PDA 10 also recovers slowly due to the low HNTs@PDA content, it is needed 246 s as for the θ of 230°. Fig. 10D displays the temperature change of hydrogels with different HNTs@PDA contents under NIR irradiation. It is obvious that the temperature rises fast for the hydrogels with HNTs@PDA, and the heating speed also gets higher with increasing HNTs@PDA content. For example, the temperature of the hydrogel of HNTs@PDA 40 rises by 34.4 °C within 10 s, but the temperature of the neat hydrogel only rises by 3.9 °C after 150 s NIR

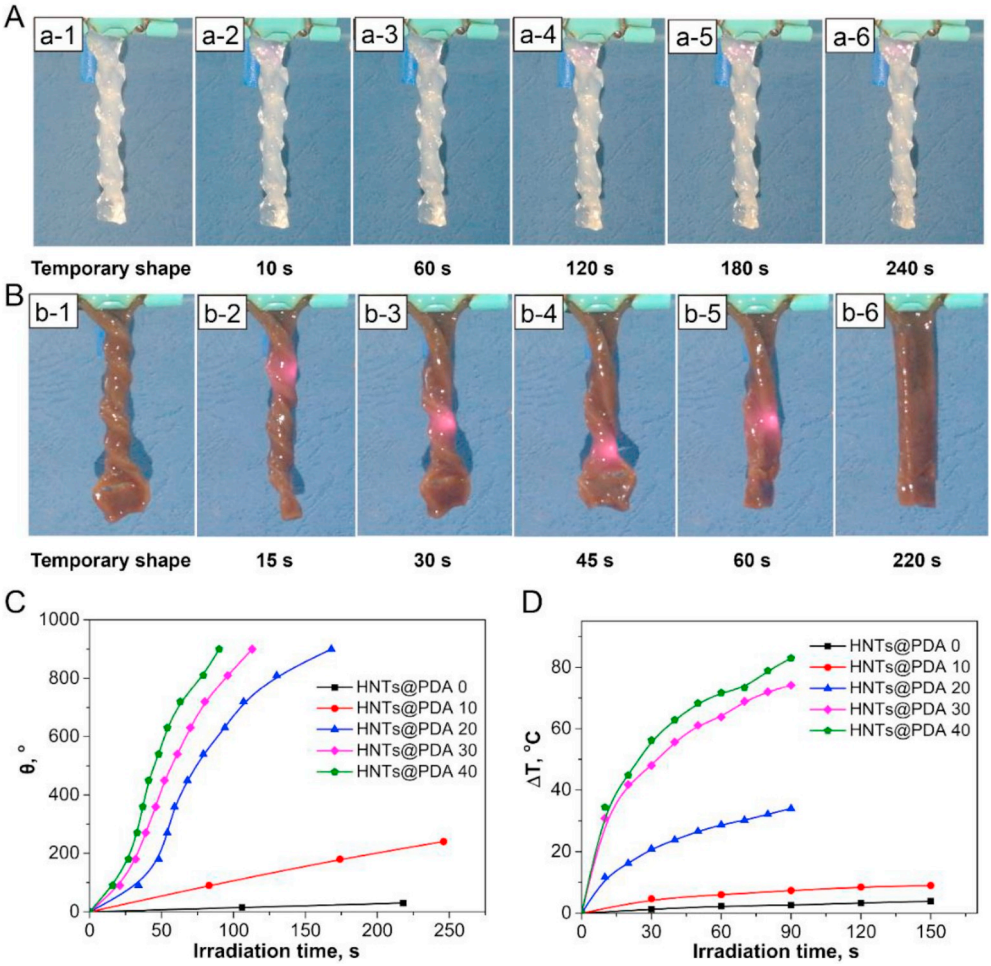

Fig. 10. (A) Shape recovery of the hydrogel without HNTs@PDA under NIR irradiation. (B) Shape recovery of the hydrogel of HNTs@PDA 40 under NIR irradiation. (C) Angle change and (D) temperature change of hydrogels with different HNTs@PDA contents under NIR irradiation.

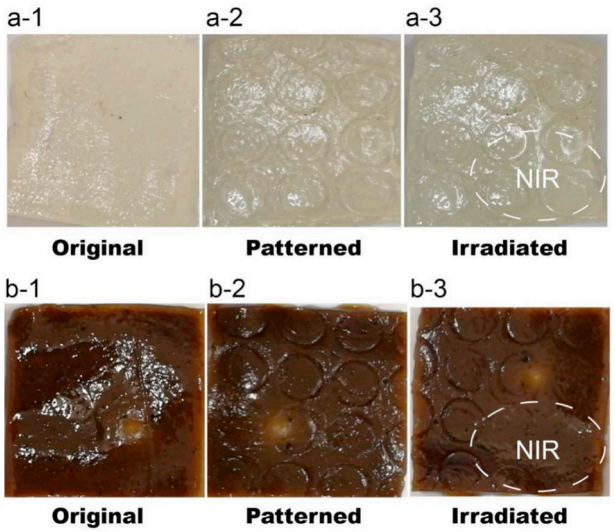

Fig. 11. (a-1, a-2 and a-3) Shape recovery of the patterned hydrogel without HNTs@PDA under NIR irradiation. (b-1, b-2 and b-3) Shape recovery of the patterned hydrogel of HNTs@PDA 40 under NIR irradiation.

light irradiation. These results also manifest the high efficiency of photothermal performance of HNTs@PDA in the hydrogel, and photothermal effect of HNTs@PDA/PAAm-Gelatin hydrogels can trigger the

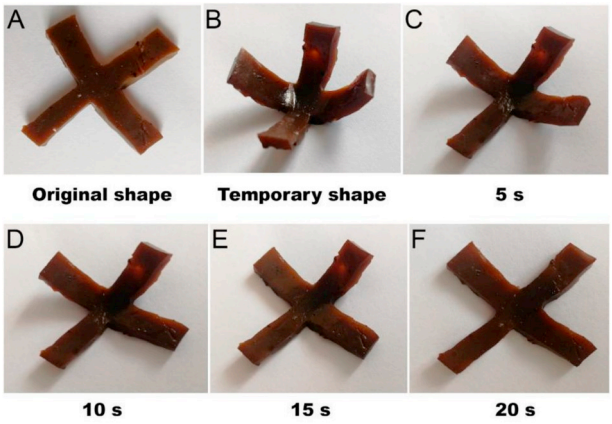

Fig. 12. Shape fixing and shape recovery images of the hydrogel of HNTs@PDA 40 under NIR irradiation.

shape recovery. Because of the heat-induced fusion of gelatin triple helix, the hydrogels are possible to recover to its permanent shape, and dense networks formed with acrylamide possess strong elastic energy which promotes to recover after curling [18].

Supplementary video related to this article can be found at https://doi.org/10.1016/j.compscitech.2020.108071.

The shape memory property of the hydrogels was also investigated

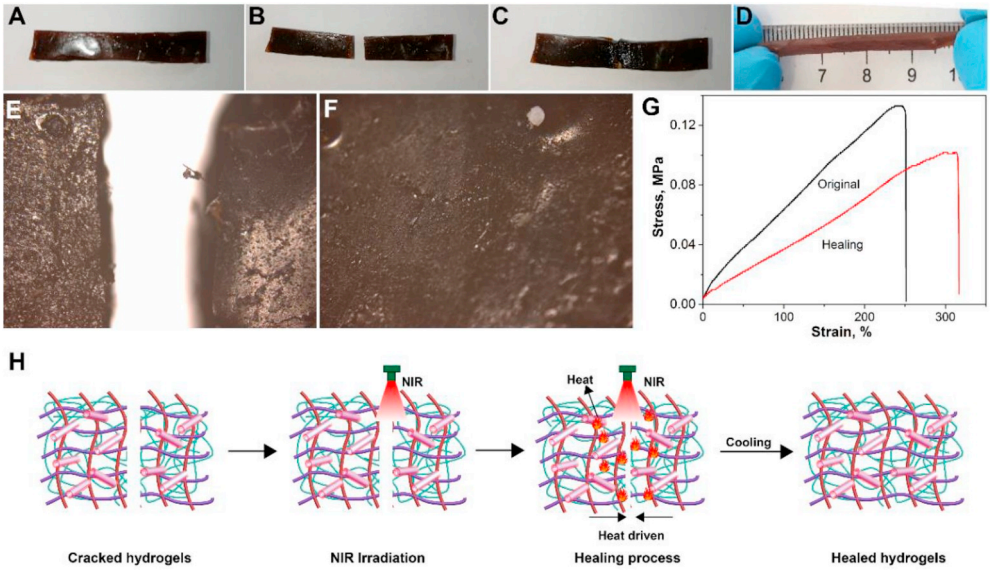

Fig. 13. Digital images of hydrogels at (A) initial state, (B) cracked state, (C) healed state and (D) stretched state after healing. The optical microscopy photos of the cut surface (E) before and (F) after NIR irradiation (output power: 2 W/cm^2, irradiation time: 3 min). (G) Stress-strain curves of initial and healed hydrogels with 40 mg/mL HNTs@PDA. (H) Schematic illustration of NIR-triggered self-healing of a cracked hydrogel.

through patterned with a multi-circle mold. From Fig. 11 a-1, a-2 and a-3, the neat hydrogel is able to keep its patterned shape and returns to its original shape slightly after NIR irradiation. In contrast, the hydrogel of HNTs@PDA 40 is also capable of maintaining the patterned shape. However, when the hydrogel is irradiated by NIR irradiation, the printed pattern of the hydrogel in the irradiated region is erased but the pattern outside this area is almost unchanged (Figs. 11 b-1, b-2 and b-3). Fig. 12 shows another shape memory phenomenon. The hydrogel of HNTs@PDA 40 was tailored to a cross shape (Fig. 12A). Then the hydrogel was first immersed into 80 °C water for 10 s and then deformed into a petal shape (Fig. 12B) which was fixed in ice water for 30 s. When the NIR light was focused at one valve of the petal, the valve recovered to its original shape fast, other valves also recovered slowly simultaneously (Fig. 12C–E). The hydrogel recovered to its original shape upon 20 s NIR light irradiation (Fig. 12F).

3.4. The self-healing behavior

The HNTs@PDA/PAAm-Gelatin hydrogels are also expected with self-healing behaviors. To study the self-healing performance, a hydrogel strip with 30 mm × 5 mm × 2 mm of HNTs@PDA 40 (Fig. 13A) was cut into two pieces (Fig. 13B) using a knife. Then the cut surfaces were immediately brought into together and irradiated by the NIR laser for 3 min to heal the damaged hydrogel. The healed hydrogel (Fig. 13C) was stretched to 50 mm (Fig. 13D) through hand, which indicates that the effect of self-healing is pretty good. The optical microscope images of the damaged and healed surfaces were presented in Fig. 13E and F, respectively. It is evidenced that the damaged surface was healed well after NIR light irradiation. The mechanical performance of the healed hydrogel is close to the original hydrogel from Fig. 13G. The tensile strength of the original hydrogel is 0.133 MPa. Then the cracked hydrogel was irradiated with NIR light and the tensile strength of the healed hydrogel is 0.101 MPa which reaches 76% of the tensile strength of the original hydrogel. These results also demonstrate that the HNTs@PDA/PAAm-Gelatin hydrogels possess excellent self-healing performance.

Fig. 13H illustrates the mechanism of NIR-triggered self-healing of a cracked hydrogel. The cracked hydrogels are exposed to NIR light and then a lot of heat which increases the temperature of the hydrogels is generated. The superior photothermal effect of the HNTs@PDA/PAAm-Gelatin hydrogels can raise the temperature at the exposed area of the hydrogel to above 100 °C. At such a high temperature, the polymer chains are free for movement. Therefore, superior photothermal effect of HNTs@PDA facilitates polymer chains to diffuse across the fracture interfaces of the hydrogel [64]. Certainly, the cracked hydrogels are healed well through NIR light-triggered effect.

4. Conclusion

HNTs@PDA was firstly synthesized through self-polymerization of dopamine on the surface of HNTs. HNTs@PDA was analyzed by various techniques, and it is found that PDA with photothermal effect was successfully coated on the surface of the tubes. The polyacrylamide-gelatin composite hydrogels reinforced by HNTs@PDA were prepared via in-situ free radical polymerization of acrylamide in the mixture of Laponite-RD, HNTs@PDA and gelatin. The tensile strength of the composite hydrogels is significantly improved. The well dispersed HNTs@PDA acts as cross-linking agent of PAAm to constitute a rigid network in the hydrogel's matrix. Furthermore, the shape recovery process of the hydrogel is quite rapid, it is required to take 63 s to recover 720° for the HNTs@PDA/PAAm-Gelatin hydrogels and the healing efficiency from tensile properties can reach 76%. The prepared PAAm composite hydrogels with NIR triggered shape memory performance and self-healing capacity show great potentials in sensors and biomedicines.

Declaration of competing interest

The authors declare that they have no known competing financial interests or personal relationships that could have appeared to influence the work reported in this paper.

CRediT authorship contribution statement

Xiang Cao: Methodology, Data curation, Investigation, Writing - original draft. **Hongzhong Liu:** Data curation. **Xiaohan Yang:** Validation. **Jinhuan Tian:** Formal analysis. **Binghong Luo:** Supervision. **Mingxian Liu:** Conceptualization, Resources, Writing - review & editing, Project administration.

Acknowledgements

This work was supported by the grants from Guangdong Basic and Applied Basic Research Foundation (2019A1515011509), and the Fundamental Research Funds for the Central Universities (21619102).

References

[1] A.M. Mathur, S.K. Moorjani, A.B. Scranton, Methods for synthesis of hydrogel networks: a review, J. Macromol. Sci. Polym. Rev. 36 (2) (1996) 405–430.
[2] A.S. Hoffman, Hydrogels for biomedical applications, Adv. Drug Deliv. Rev. 64 (2012) 18–23.
[3] M.R. Guilherme, F.A. Aouada, A.R. Fajardo, A.F. Martins, A.T. Paulino, M.F. Davi, A.F. Rubira, E.C. Muniz, Superabsorbent hydrogels based on polysaccharides for application in agriculture as soil conditioner and nutrient carrier: a review, Eur. Polym. J. 72 (2015) 365–385.
[4] C.Y. Anthony, H. Chen, D. Chan, G. Agmon, L.M. Stapleton, A.M. Sevit, M. W. Tibbitt, J.D. Acosta, T. Zhang, P.W. Franzia, Scalable manufacturing of biomimetic moldable hydrogels for industrial applications, Proc. Natl. Acad. Sci. Unit. States Am. 113 (50) (2016) 14255–14260.
[5] K.Y. Lee, D.J. Mooney, Hydrogels for tissue engineering, Chem. Rev. 101 (7) (2001) 1869–1880.
[6] J. Li, D.J. Mooney, Designing hydrogels for controlled drug delivery, Nat. Rev. Mater. 1 (12) (2016) 16071.
[7] X. Zhao, H. Wu, B. Guo, R. Dong, Y. Qiu, P.X. Ma, Antibacterial anti-oxidant electroactive injectable hydrogel as self-healing wound dressing with hemostasis and adhesiveness for cutaneous wound healing, Biomaterials 122 (2017) 34–47.
[8] L. Li, Y. Wang, L. Pan, Y. Shi, W. Cheng, Y. Shi, G. Yu, A nanostructured conductive hydrogels-based biosensor platform for human metabolite detection, Nano Lett. 15 (2) (2015) 1146–1151.
[9] X. Zhao, Q. Lang, L. Yildirimer, Z.Y. Lin, W. Cui, N. Annabi, K.W. Ng, M. R. Dokmeci, A.M. Ghaemmaghami, A. Khademhosseini, Photocrosslinkable gelatin hydrogel for epidermal tissue engineering, Adv. Healthc. Mater. 5 (1) (2016) 108–118.
[10] E.A. Naumenko, I.D. Guryanov, R. Yendluri, Y.M. Lvov, R.F. Fakhrullin, Clay nanotube-biopolymer composite scaffolds for tissue engineering, Nanoscale 8 (13) (2016) 7257–7271.
[11] S.S. Suner, S. Demirci, B. Yetiskin, R. Fakhrullin, E. Naumenko, O. Okay, R. S. Ayyala, N. Sahiner, Cryogel composites based on hyaluronic acid and halloysite nanotubes as scaffold for tissue engineering, Int. J. Biol. Macromol. 130 (2019) 627–635.
[12] A.S. Hoffman, Environmentally sensitive polymers and hydrogels, MRS Bull. 16 (9) (1991) 42–46.
[13] B. Zhao, J.S. Moore, Fast pH-and ionic strength-responsive hydrogels in microchannels, Langmuir 17 (16) (2001) 4758–4763.
[14] F.-J. Xu, E.-T. Kang, K.-G. Neoh, pH- and temperature-responsive hydrogels from crosslinked triblock copolymers prepared via consecutive atom transfer radical polymerizations, Biomaterials 27 (14) (2006) 2787–2797.
[15] Y.-L. Zhao, J.F. Stoddart, Azobenzene-based light-responsive hydrogel system, Langmuir 25 (15) (2009) 8442–8446.
[16] P. Gupta, K. Vermani, S. Garg, Hydrogels: from controlled release to pH-responsive drug delivery, Drug Discov. Today 7 (10) (2002) 569–579.
[17] M. Hamidi, A. Azadi, P. Rafiei, Hydrogel nanoparticles in drug delivery, Adv. Drug Deliv. Rev. 60 (15) (2008) 1638–1649.
[18] J. Huang, L. Zhao, T. Wang, W. Sun, Z. Tong, NIR-triggered rapid shape memory PAM-GO-gelatin hydrogels with high mechanical strength, ACS Appl. Mater. Interfaces 8 (19) (2016) 12384–12392.
[19] C. Hou, Y. Duan, Q. Zhang, H. Wang, Y. Li, Bio-applicable and electroactive near-infrared laser-triggered self-healing hydrogels based on graphene networks, J. Mater. Chem. 22 (30) (2012) 14991–14996.
[20] Y.M. Lvov, D.G. Shchukin, H. Mohwald, R.R. Price, Halloysite clay nanotubes for controlled release of protective agents, ACS Nano 2 (5) (2008) 814–820.
[21] M. Liu, Z. Jia, D. Jia, C. Zhou, Recent advance in research on halloysite nanotubes-polymer nanocomposite, Prog. Polym. Sci. 39 (8) (2014) 1498–1525.
[22] E. Joussein, S. Petit, J. Churchman, B. Theng, D. Righi, B. Delvaux, Halloysite clay minerals-a review, Clay Miner. (2005) 383–426.
[23] D. Lu, H. Chen, J. Wu, C.M. Chan, Direct measurements of the Young's modulus of a single halloysite nanotube using a transmission electron microscope with a bending stage, J. Nanosci. Nanotechnol. 11 (9) (2011) 7789–7793.
[24] Y. Lvov, E. Abdullayev, Functional polymer-clay nanotube composites with sustained release of chemical agents, Prog. Polym. Sci. 38 (10–11) (2013) 1690–1719.
[25] N.F.A. Sharif, Z. Mohamad, A. Hassan, M.U. Wahit, Novel epoxidized natural rubber toughened polyamide 6/halloysite nanotubes nanocomposites, J. Polym. Res. 19 (1) (2012) 9749.
[26] M. Albdiry, H. Ku, B. Yousif, Impact fracture behaviour of silane-treated halloysite nanotubes-reinforced unsaturated polyester, Eng. Fail. Anal. 35 (2013) 718–725.
[27] Y. Ye, H. Chen, J. Wu, C.M. Chan, Interlaminar properties of carbon fiber composites with halloysite nanotube-toughened epoxy matrix, Compos. Sci. Technol. 71 (5) (2011) 717–723.
[28] D. Fix, D.V. Andreeva, Y.M. Lvov, D.G. Shchukin, H. Möhwald, Application of inhibitor-loaded halloysite nanotubes in active anti-corrosive coatings, Adv. Funct. Mater. 19 (11) (2009) 1720–1727.
[29] M. Du, B. Guo, M. Liu, D. Jia, Formation of reinforcing inorganic network in polymer via hydrogen bonding self-assembly process, Polym. J. 39 (3) (2007) 208.
[30] M. Liu, B. Guo, M. Du, X. Cai, D. Jia, Properties of halloysite nanotube-epoxy resin hybrids and the interfacial reactions in the systems, Nanotechnology 18 (45) (2007) 455703.
[31] M. Du, B. Guo, Y. Lei, M. Liu, D. Jia, Carboxylated butadiene-styrene rubber/halloysite nanotube nanocomposites: interfacial interaction and performance, Polymer 49 (22) (2008) 4871–4876.
[32] M. Du, B. Guo, D. Jia, Newly emerging applications of halloysite nanotubes: a review, Polym. Int. 59 (5) (2010) 574–582.
[33] Q. Peng, M. Liu, J. Zheng, C. Zhou, Adsorption of dyes in aqueous solutions by chitosan-halloysite nanotubes composite hydrogel beads, Microporous Mesoporous Mater. 201 (2015) 190–201.
[34] Y. Zheng, A. Wang, Enhanced adsorption of ammonium using hydrogel composites based on chitosan and halloysite, J. Macromol. Sci., Part A 47 (1) (2009) 33–38.
[35] B. Huang, M. Liu, C. Zhou, Cellulose-halloysite nanotube composite hydrogels for curcumin delivery, Cellulose 24 (7) (2017) 2861–2875.
[36] M. Liu, Y. Zhang, J. Li, C. Zhou, Chitin-natural clay nanotubes hybrid hydrogel, Int. J. Biol. Macromol. 58 (2013) 23–30.
[37] B. Huang, M. Liu, Z. Long, Y. Shen, C. Zhou, Effects of halloysite nanotubes on physical properties and cytocompatibility of alginate composite hydrogels, Mater. Sci. Eng. C 70 (2017) 303–310.
[38] M. Liu, W. Li, J. Rong, C. Zhou, Novel polymer nanocomposite hydrogel with natural clay nanotubes, Colloid Polym. Sci. 290 (10) (2012) 895–905.
[39] B. Huang, M. Liu, C. Zhou, Chitosan composite hydrogels reinforced with natural clay nanotubes, Carbohydr. Polym. 175 (2017) 689–698.
[40] A.D. Hughes, M.R. King, Use of naturally occurring halloysite nanotubes for enhanced capture of flowing cells, Langmuir 26 (14) (2010) 12155–12164.
[41] R. He, M. Liu, Y. Shen, Z. Long, C. Zhou, Large-area assembly of halloysite nanotubes for enhancing the capture of tumor cells, J. Mater. Chem. B 5 (9) (2017) 1712–1723.
[42] V. Vergaro, E. Abdullayev, Y.M. Lvov, A. Zeitoun, R. Cingolani, R. Rinaldi, S. Leporatti, Cytocompatibility and uptake of halloysite clay nanotubes, Biomacromolecules 11 (3) (2010) 820–826.
[43] M. Liu, Y. Shen, P. Ao, L. Dai, Z. Liu, C. Zhou, The improvement of hemostatic and wound healing property of chitosan by halloysite nanotubes, RSC Adv. 4 (45) (2014) 23540–23553.
[44] Y.M. Lvov, M.M. DeVilliers, R.F. Fakhrullin, The application of halloysite tubule nanoclay in drug delivery, Expet Opin. Drug Deliv. 13 (7) (2016) 977–986.
[45] R. Qi, R. Guo, F. Zheng, H. Liu, J. Yu, X. Shi, Controlled release and antibacterial activity of antibiotic-loaded electrospun halloysite/poly (lactic-co-glycolic acid) composite nanofibers, Colloids Surf. B Biointerfaces 110 (2013) 148–155.
[46] G. Cavallaro, G. Lazzara, S. Milioto, F. Parisi, V. Evtugyn, E. Rozhina, R.J.A.a. m. Fakhrullin, interfaces, Nanohydrogel formation within the halloysite lumen for triggered and sustained release, ACS Appl. Mater. Interfaces 10 (9) (2018) 8265–8273.
[47] A. Panchal, G. Fakhrullina, R. Fakhrullin, Y. Lvov, Self-assembly of clay nanotubes on hair surface for medical and cosmetic formulations, Nanoscale 10 (38) (2018) 18205–18216.
[48] D.R. Dreyer, D.J. Miller, B.D. Freeman, D.R. Paul, C.W. Bielawski, Elucidating the structure of polydopamine, Langmuir 28 (15) (2012) 6428–6435.
[49] X. Zeng, M. Luo, G. Liu, X. Wang, W. Tao, Y. Lin, X. Ji, L. Nie, L. Mei, Polydopamine-modified black phosphorous nanocapsule with enhanced stability and photothermal performance for tumor multimodal treatments, Adv. Sci. 5 (10) (2018) 1800510.
[50] Z. Li, X. Zhang, S. Wang, Y. Yang, B. Qin, K. Wang, T. Xie, Y. Wei, Y. Ji, Polydopamine coated shape memory polymer: enabling light triggered shape recovery, light controlled shape reprogramming and surface functionalization, Chem. Sci. 7 (7) (2016) 4741–4747.
[51] Y. Liu, K. Ai, J. Liu, M. Deng, Y. He, L. Lu, Dopamine-melanin colloidal nanospheres: an efficient near-infrared photothermal therapeutic agent for in vivo cancer therapy, Adv. Mater. 25 (9) (2013) 1353–1359.
[52] L. Yang, Z. Wang, G. Fei, H. Xia, Polydopamine particles reinforced poly (vinyl alcohol) hydrogel with NIR light triggered shape memory and self-healing capability, Macromol. Rapid Commun. 38 (23) (2017) 1700421.
[53] K. Feng, G.-Y. Hung, X. Yang, M. Liu, High-strength and physical cross-linked nanocomposite hydrogel with clay nanotubes for strain sensor and dye adsorption application, Compos. Sci. Technol. (2019) 107701.
[54] J. Zhang, X. Luo, Y.-P. Wu, F. Wu, Y.-F. Li, R.-R. He, M. Liu, Rod in tube: a novel nanoplatform for highly effective chemo-photothermal combination therapy toward breast cancer, ACS Appl. Mater. Interfaces 11 (4) (2019) 3690–3703.
[55] Y. Liu, M. Liu, Conductive carboxylated styrene butadiene rubber composites by incorporation of polypyrrole-wrapped halloysite nanotubes, Compos. Sci. Technol. 143 (2017) 56–66.
[56] S. Lin, C.T. Chen, I. Bdikin, V. Ball, J. Grácio, M.J. Buehler, Tuning heterogeneous polydopamine structures and mechanics: in silico covalent cross-linking and thin film nanoindentation, Soft Matter 10 (3) (2013) 457–464.
[57] N.F.D. Vecchia, R. Avolio, M. Alfè, M.E. Errico, A. Napolitano, M. D'Ischia, Building-block diversity in polydopamine underpins a multifunctional eumelanin-type platform tunable through a quinone control point, Adv. Funct. Mater. 23 (10) (2013) 1331–1340.
[58] J. Madejová, FTIR techniques in clay mineral studies, Vib. Spectrosc. 31(1) 1-10.
[59] F. Wu, J. Zheng, Z. Li, M. Liu, Halloysite nanotubes coated 3D printed PLA pattern for guiding human mesenchymal stem cells (hMSCs) orientation, Chem. Eng. J. 359 (2019) 672–683.

[60] J. Zhang, T. Liu, M. Liu, Hydrothermal synthesis of halloysite nanotubes@ carbon nanocomposites with good biocompatibility, Microporous Mesoporous Mater. 266 (2018) 155–163.
[61] J. Ahmed, M. Mulla, A. Joseph, M. Ejaz, M. Maniruzzaman, Zinc oxide/clove essential oil incorporated type B gelatin nanocomposite formulations: a proof-of-concept study for 3D printing applications, Food Hydrocolloids 98 (2020) 105256.
[62] G. Brindley, K. Robinson, D. MacEwan, The clay minerals halloysite and meta-halloysite, Nature 157 (3982) (1946) 225.
[63] H.L.K. Haraguchi, K. Matsuda, T. Takehisa, E. Elliott, Mechanism of forming organic/inorganic network structures during in-situ free-radical polymerization in PNIPA-clay nanocomposite hydrogels, Macromolecules 38 (8) (2005) 3482–3490.
[64] E. Zhang, T. Wang, L. Zhao, W. Sun, X. Liu, Z. Tong, Fast self-healing of graphene oxide-hectorite clay-poly (N, N-dimethylacrylamide) hybrid hydrogels realized by near-infrared irradiation, ACS Appl. Mater. Interfaces 6 (24) (2014) 22855–22861.